Development of an Uncertainty Model for the National Transonic Facility (Invited)

Joel A. Walter[1], William R. Lawrence[2], and David W. Elder[3]
Jacobs Technology, Inc, Tullahoma, TN 37388.

and

Michael D. Treece[4]
Analytical Services and Materials, Inc., Hampton VA 23681

This paper introduces an uncertainty model being developed for the National Transonic Facility (NTF). The model uses a Monte Carlo technique to propagate standard uncertainties of measured values through the NTF data reduction equations to calculate the combined uncertainties of the key aerodynamic force and moment coefficients and freestream properties. The uncertainty propagation approach to assessing data variability is compared with ongoing data quality assessment activities at the NTF, notably check standard testing using statistical process control (SPC) techniques. It is shown that the two approaches are complementary and both are necessary tools for data quality assessment and improvement activities. The SPC approach is the final arbiter of variability in a facility. Its result encompasses variation due to people, processes, test equipment, and test article. The uncertainty propagation approach is limited mainly to the data reduction process. However, it is useful because it helps to assess the causes of variability seen in the data and consequently provides a basis for improvement. For example, it is shown that Mach number random uncertainty is dominated by static pressure variation over most of the dynamic pressure range tested. However, the random uncertainty in the drag coefficient is generally dominated by axial and normal force uncertainty with much less contribution from freestream conditions.

Nomenclature

C_A	axial force coefficient		
C_D	drag coefficient	Re_c	chord Reynolds number
C_L	lift coefficient	T_s, T_t	static and total temperature
C_N	normal force coefficient	u	standard uncertainty
F_N	normal force	u_c	combined standard uncertainty
F_A	axial force	$U = ku_c$	expanded uncertainty
M_∞	freestream Mach number	W	molecular weight
k	coverage factor	x	a measured quantity
q_∞	freestream dynamic pressure	y	result of a data reduction equation
P_s, P_t	static and total pressure	α	angle of attack
R	universal gas constant	ρ_s	static density
S	reference area	σ_{wg}	estimated within-group standard deviation
LN2	liquid nitrogen	2σ	expanded uncertainty with $k = 2$

[1] Senior Engineer, Technology Group, Bingham Farms, MI 48025. AIAA Senior Member.
[2] Technical Fellow - Aerodynamics, ATA Group, Tullahoma, TN 37389.
[3] Manager, Instrumentation and Data Acquisition Services, ROME Group, Hampton VA 23666.
[4] Test Engineer, ROME Group, Hampton VA 23681. AIAA Member.

I. Introduction

Competitive and environmental concerns are driving unprecedented levels of product performance requirements at minimum development cost, and aerodynamic performance is no exception. Fuel economy is a relevant example. For a commercial aircraft program, fuel economy targets dictated either by customer or environmental constraints may drive the selection of an aggressive wing design that optimizes drag at cruise condition, but which carries some risk at an off-design condition, e.g., excessive trailing-edge boundary layer separation. The aerodynamicist needs high confidence in his predictions of in-flight aerodynamic performance at both conditions if his recommendations for the cruise condition carry with them performance risk at another condition. An automobile development program will routinely be under regulatory pressure to achieve a difficult design target for fuel economy, with consumer pressure not to compromise styling and cabin room, both while ensuring adequate engine cooling flow and safe handling characteristics. Hundreds of hours of wind tunnel time and even more computer time will be expended, from the first reduced-scale clay model to the final pre-production prototype, to achieve a series of small aerodynamic improvements. Taken alone, any one of these may account for only a few tenths of a mile per gallon. Taken together, they may provide a significant improvement but many of them add cost to the final product. Again, the aerodynamicist needs an accurate understanding of each modification's influence on fuel economy in real-world driving conditions if his design recommendations are going to result in increasing the vehicle's cost to manufacture.

In the past, a more conservative approach would likely have been taken in both examples, because the lower confidence level in the available design data would not have been able to mitigate the performance risk of the aggressive wing design or justify the additional program cost for the aerodynamic enhancements to the automobile. The resulting compromises that in the past would have been acceptable from a commercial or regulatory standpoint would no longer be acceptable. In this setting – where performance requirements tighten but program budgets decrease – the need is evident for high-fidelity data with which to make the right design decisions. This has implications for aerodynamic development tools. Techniques that were previously used primarily for research or concept development must be transitioned faster into providing design direction; tools that previously provided design direction now need to give high-precision answers that closely resemble free-air conditions. And prototype or flight testing has to be minimized as much as possible to contain program cost and thus the end customer's cost. This trend means, for example, that computational methods are being relied upon deeper into the product development process, and design decisions from experimental results – primarily wind tunnel tests – are being made on the basis of ever-smaller observations of performance increments.

This product development environment requires a structured and ongoing internal commitment to maintaining data quality: methods to assess overall tunnel performance[1] along with analytical tools[2-4], processes, training, and commitment of resources (especially tunnel time) to diagnose and understand the causes of data variability at the subsystem level. Through these activities, it is possible to define and pursue opportunities for continuous improvement in both the precision (repeatability) and accuracy (fidelity relative to free-air conditions) of the simulations provided to the customer.

The purpose of this paper is to report on additional progress at the National Transonic Facility (NTF) toward enhancing data quality by introducing and exercising a comprehensive numerical model to assess data uncertainty at the NTF. Section II places this paper in context relative to other continuous improvement activities at the NTF. In Section III, we provide a high-level review of methods for estimating variability, as a means of both introducing the model and placing it in context relative to previous work at NTF in this area. We describe the numerical model in detail Section IV, the benchmark tests used to populate it in Section V, and present some results in Section VI.

II. Data Quality Assessment at the NTF

The National Transonic Facility[5] is a high-Reynolds number transonic wind tunnel capable of varying Mach number, Reynolds number, and dynamic pressure independently by pressurizing the circuit and operating in cryogenic (nitrogen) or warm air mode. It has a unique potential to provide the high-fidelity design data required in the product development environment just described. On the other hand, a cursory review of the literature describing its conception and development, even up to the time it became operational[6], suggests that it was intended primarily as a research facility. Further, the NTF was the first of its kind to be built at large scale, and remains today the largest cryogenic wind tunnel in the world. This means that part of its initial mission necessarily became how to operate and maintain a large cryogenic wind tunnel.[7,8] Although the NTF remains an essential national asset for high Reynolds number research, activities are ongoing[1,9,10] to address the data quality features mentioned above that are now necessary for product development testing.

In addition to data quality concerns, productivity and reliability enhancements must also be addressed continually. In that regard, several initiatives have been completed recently or are currently underway to assess and improve the productivity and reliability of the NTF. An on-site LN2 plant was completed in 2008. It produces more than 1.5 times the amount of LN2 than could be provided previously and allows the tanks to be filled while the tunnel continues to run. A full upgrade of the NTF control and data systems is currently in progress. The control system is being replaced with a modern, programmable system. The new data system will provide a 5-fold increase in throughput, a 4-fold increase in the scan rate, and it will double the number of A/D channels, all of which will have 16-bit resolution. The calculation base will be converted entirely to a commercial off-the-shelf product with time-aligned input signals so that continuous-sweep data acquisition and reduction is possible.

III. Estimating Data Variability

Several previous investigations at the NTF have either focused on uncertainty analysis or included elements of it. This section provides an overview of several approaches to characterizing data variability with particular emphasis on past work at the NTF. It is neither exhaustive nor rigorous, but rather an attempt to explain and then compare, in simple terms, the relative strengths and weaknesses of the different approaches.

A. Regression Statistical Analysis (RSA)

Wahls et al.[11] investigated primarily short-term (within-test) variability on a commercial transport model. Mineck and Pendergraft[12] used a similar analytical approach but with focus on test-to-test variability. They used classical multiple linear regression techniques to characterize spread in the results. Their approach was to use monomials as basis functions from one set of measured data (such as angle of attack) to develop regressions that provide the best fit to another measured variable (such as lift coefficient). In particular, they formed a single best-estimate curve fit from combined sets of identical runs. They referred to this approach as Regression Statistical Analysis (RSA). An example is shown in Fig. 1. A statistical estimate of variability is obtained with this approach by calculating either the confidence interval or prediction interval (which is shown in the figure). Both are functions of the standard error the fit, the local data density, and the *t*-statistic for the desired confidence level. The confidence interval estimates the bounds within which the true mean is likely to fall, at the specified level of confidence. The prediction interval indicates the band within which a single future observation can be expected fall, at the specified level of confidence. The prediction interval seems more appropriate in most cases – in practice, the technique is used while the test is progressing to make sure repeat runs don't show any surprises.

While the RSA fit provides a metric to assess variability, it lacks somewhat in rigor. For example, unless variances (uncertainties) are specified for each dependent variable in the fit, there is no way to assess the quality of the model[13] itself (i.e., 4th order polynomials in the case Fig. 1), so the choice of basis functions to use is arbitrary, although rules of thumb[11] and past experience certainly provide guidance. In addition, standard regression techniques assume no variability in the dependent variable, which is clearly not the case when a measured parameter is used. As a result, Fig. 1 shows that the prediction interval for the same independent variable (C_D) differs by almost a factor of 2 when α is used for the dependent variable instead of C_L. In spite of these drawbacks, the RSA approach is a quick and visual method to obtain an estimate of variability and only requires data that are available as the test progresses.

B. Statistical Process Control (SPC)

A long-term initiative at the Langley Research Center, led by Hemsch[1,9,14] and co-workers, has resulted in an established data quality assurance program at the NTF and other Langley wind tunnels. It is based on Shewhart control charts to monitor and maintain statistical process control (SPC) of the key aerodynamic force and moment coefficients. SPC techniques have a long and well-vetted history of application across many different disciplines[15], most notably as a tool for quality control in manufacturing. For wind tunnel applications in particular, Hemsch et al.[14] provide an excellent introduction to the topic in general and describe the check standard programs they designed to balance economic and technical considerations. A subsequent paper[9] focused on the NTF specifically, showing initial results of the approach from three separate tests.

Fig. 2 shows a process control chart for the axial force coefficient C_A on the NTF's Pathfinder I transport model[16] check standard. This chart contains data from 2004-2010. The top chart shows the group average and the bottom chart shows the group range. A 'group' in this case is the two measurements of C_A at the common test conditions shown in the caption. Each measurement is one point in a pitch polar run, and between these two runs are back-to-back inverted pitch polar runs. Separate groups on the chart represent either a different test series (i.e., a

subsequent repeat of the pitch polar after a data set at different freestream conditions has been measured) or a different test (installation) altogether.

In Fig. 2, the estimated in-group variability is about $2\sigma_{wg} = \pm 0.0001$, or 1 count of drag for a transport model. A coverage factor of is 2 applied to σ_{wg}, which is traditionally considered to approximate a 95% confidence level. The group average data fall within the upper and lower control limits on the chart, so the process being measured may be said to be 'in statistical control.' Whether the resulting estimated variability is *satisfactory* is a different question, which is answered, of course, by considering the variability in relation to customer requirements.

Establishing and maintaining a process control program is arguably the most important aspect of a wind tunnel's data quality assurance program. The data are used to define the control limits, so the control chart rigorously defines the tunnel's variability. It is not confined to repeatability (as is RSA) nor to the data reduction process (as is uncertainty propagation discussed below), but instead includes all sources of variability in the tunnel operation – people, processes, equipment, and test article. However, such programs are also expensive because regular tunnel entries are required; this is amplified for tunnels with a large operating envelope and a diversity of test articles. Even so, SPC programs are the only way to monitor the actual variability of the tunnel, and demonstrate this to the customer so that he can assign appropriate confidence to his own results when making product decisions.

It is difficult with SPC techniques to drill down into the variability – to answer the question of *why* the variability exhibits the levels it does. The very rigor of the method requires that new tests be designed and new data acquired and analyzed to answer the question. The uncertainty propagation method described next helps to answer the question, but at the expense in some cases of replacing measured data and statistical rigor with engineering judgment.

C. Uncertainty Propagation

1. Definitions

Up to this point, we have avoided as much as possible using terms like error, accuracy, and uncertainty, instead using (and conveniently neglecting to define) the term variability. Accuracy is the closeness of agreement between a measurement result and its true value. However, the true value is not known, nor can it be, so it follows that accuracy is only a qualitative term. Similarly, error is the degree of inaccuracy, i.e., the difference between the measured result and true value, so it too is unknowable and thus qualitative. Uncertainty is a quantified estimate of the error, hopefully based on a statistical analysis of measured data, but, when necessary for economic or other reasons, based on experience and judgment. These notions are based on the definitions given in the ISO *Guide to the Expression of Uncertainty in Measurement*[17].

It is often helpful in understanding and analyzing error sources to classify them. A common approach is to classify errors as random or systematic, also known as precision and bias errors, respectively. The simple definitions for these terms are that a random error contributes to data scatter whereas a systematic error does not[18].

Systematic errors sources are usually related to residual error after calibration, data acquisition methods, operator interaction (deciding when the tunnel is 'on point'), conceptual errors (measuring a distorted artifact of what was intended) and math models used to adjust data (e.g., blockage corrections). Random error is related to the scatter of successive measurements that are made under nominally identical conditions. It results from randomly occurring factors in the measurement system that cannot be identified and/or controlled. If such factors could be identified and controlled or eliminated, then the random error would be reduced.

The classification of errors as random or systematic is context-specific and must be considered carefully in each situation. For example, a transducer output during calibration may be subject to random variations due to uncontrolled environmental changes in the laboratory. But that random error is fossilized[19] into the calibration's gain coefficient, so it is a systematic error in the context of the wind tunnel's use of the transducer. Conversely, test article misalignment is a fixed systematic error for any one test article installation, but viewed across installations it is a random error in the sense that it contributes to data scatter. The ISO *Guide*[17] recommends against the classification of errors as random or systematic because of ambiguities such as these, and also because there is fundamentally no difference in how the uncertainties are combined and used in subsequent uncertainty calculations. However, we retain the systematic and random terminology in this paper as a helpful tool to identify and classify error sources, even if the classifications sometimes contain ambiguities.

2. Propagation Equation

The method of uncertainty propagation estimates the error in a calculated measurement result by propagating estimated errors in the measured quantities through the data reduction equation that leads to that result. The uncertainty propagation equation is derived as a linearized Taylor series expansion about the true result. The true

result is then replaced by its estimate – the sum of the measured result and the error estimates (uncertainties). Ref. 20 provides a complete derivation. The *Guide*[17] defines the standard uncertainty u as an estimate for the standard deviation of a measured quantity. The uncertainty propagation equation is used to determine the combined standard uncertainty u_c of a result that is calculated from measured quantities. For a result y that is calculated as a function of N measured variables x_i, the combined standard uncertainty is the square root of the combined variance u_c^2:

$$\begin{aligned} u_c^2(y) &= \sum_{i=1}^{N} \sum_{j=1}^{N} \frac{\partial y}{\partial x_i} \frac{\partial y}{\partial x_i} u(x_i, x_j) \\ &= \sum_{i=1}^{N} \left(\frac{\partial y}{\partial x_i} \right)^2 u^2(x_i) + 2 \sum_{i=1}^{N-1} \sum_{j=i+1}^{N} \frac{\partial y}{\partial x_i} \frac{\partial y}{\partial x_i} u(x_i, x_j) \end{aligned} \tag{1}$$

The second term accounts for correlations between the measurements x_i, as, for example, in the case of two transducers that would inherit a common portion of their uncertainty if both had been calibrated previously against the same standard.

As a simple example, the density of an ideal gas is a function of the pressure, temperature, the universal gas constant, and the molecular weight of the gas:

$$\rho_s = \frac{P_s}{(R/W)T_s} \tag{2}$$

The standard uncertainty (ignoring correlated terms for the moment) is

$$\begin{aligned} u_{c,\rho_s} &= \sqrt{\left(u_{P_s} \frac{\partial \rho_s}{\partial P_s} \right)^2 + \left(u_W \frac{\partial \rho_s}{\partial W} \right)^2 + \left(u_R \frac{\partial \rho_s}{\partial R} \right)^2 + \left(u_{T_s} \frac{\partial \rho_s}{\partial_{T_s}} \right)^2} \\ &= \sqrt{\left(u_{P_s} \frac{W}{RT_s} \right)^2 + \left(u_W \frac{P_s}{RT_s} \right)^2 + \left(u_R \frac{-P_s W}{R^2 T_s} \right)^2 + \left(u_{T_s} \frac{-P_s W}{RT_s^2} \right)^2} \end{aligned} \tag{3}$$

We will compare Eq. (3) to its equivalent formulation as a Monte Carlo simulation later in the paper.

3. Coverage Factor

A coverage factor k is usually applied to the standard uncertainty to obtain the expanded or overall uncertainty as $U = ku_c$. The purpose of the coverage factor is to provide an interval about y that can be expected to encompass 'most' measurement results likely to be realized, so that the final result is expressed as $Y = y \pm U$. Equation (1) requires no assumptions about the underlying probability distributions of the errors in $u(x_i)$. However, when k is chosen, it brings an implicit assumption about the nature of these distributions[20]. A value of $k = 2$ or 3 is common; if the errors in x_i from Eq. (1) are normally distributed, $k = 2$ corresponds approximately to a 95% confidence level. In the remainder of the paper, where we refer to a "2σ uncertainty," it should be taken to mean the expanded uncertainty with $k = 2$.

D. Comparison of the Approaches to Estimating Variability

The three approaches to quantifying data variability discussed above are not in competition; in fact, all three are important because of their unique advantages. The uncertainty propagation approach is the only practical way to drill into the data reduction equations to get a sense of what error sources are likely to dominate at different conditions in the operating envelope. This provides an analytical basis for justifying continuous improvement initiatives, and can provide customers with a pre-test estimate of uncertainties they can expect for test conditions that are not close to those used in the regular benchmark entries. But it is limited to the data reduction process: it does not model how trip strips are applied and checked from one entry to the next, nor does it account for lunch breaks, shift changes, leaking valves, or loose cable connections. The SPC approach provides feedback on the overall facility performance (people, processes, and equipment) to both customers and operations staff. With its

firm statistical grounding, its answer over time—the 'Voice of the Process'—is the final arbiter in quantifying the variability of key facility parameters as well as whether the facility operation is 'in control.' It is expensive – it requires regular entries to sample the process – but it is critical to the success of a production test facility. Finally, the RSA approach is very quick and visual, and it requires only the test data at hand to get an estimate of the data variability. It is the least rigorous of the three approaches, but the reality is that any estimate of variability that can be had in near real-time is useful.

IV. Data Reduction and Uncertainty Analysis Programs for the NTF

The uncertainty model for the NTF is based on a Monte Carlo simulation technique, which is in turn wrapped around an offline NTF data reduction model. The uncertainty model propagates the standard uncertainties of measured data (P_t, P_s, etc.) through the NTF data reduction algorithm to generate combined standard uncertainties of the calculated parameters (C_D, C_L, etc.).

A. Offline Data Reduction

The offline data reduction program for the NTF is a Matlab implementation that replicates most of the online data reduction process described in Ref. 21 along with several modifications made since then. The translation was originally conceived as a general tool to model the balance data reduction equations in several Langley wind tunnels. Subsequent work incorporated the real gas model and calculation of freestream properties so that aerodynamic force and moment coefficients could be calculated. When it was decided to extend the model's use for uncertainty propagation, the various routines were vectorized as much as possible, which improved the data reduction time by about an order of magnitude. (A Monte Carlo simulation with 10,000 iterations takes a few seconds on a laptop PC.) The calculation starts with data that have already been averaged and converted to engineering units, but the model will eventually extend back to raw count data.

B. Uncertainty Analysis Using Monte Carlo Numerical Simulation

Coleman and Steele[20] describe the application of Monte Carlo simulation techniques applied to uncertainty analysis and provide several references to its use in developing or validating concepts such as assessing the quality of the coverage factor for small-sample analyses. The approach has also been applied previously in automotive wind tunnel and related applications by Walter and co-authors[4,22] and by others in numerous applications outside of aerodynamics.

A Monte Carlo simulation generates a synthetic population of test results. The data reduction algorithm is executed numerous (i.e., several hundred or thousand or more) times, with the measurands randomly perturbed on each iteration. The technique can use actual test data to represent the entire population of such measurements. The underlying assumption is that the errors do not vary rapidly as a function of the true result[13], so a single physical realization can serve as a reasonable surrogate for the true result for the purpose of comparing it to synthetically-generated results. The simulation provides a synthetic population of 'experimental' results, whose standard deviation is taken as the combined standard uncertainty.

As a simple example, the following pseudocode is the equivalent to the ideal-gas density data reduction and uncertainty given in Eqs. (2) and (3):

```
% Experimental data – surrogate for the 'true' result
T = 15 + 273.15;    P = 101325;  R = 8314.47215;      W = 28.9644;

% standard uncertainties
stdUncT = 0.5;   stdUncP = 50;   stdUncR = 0.9e-03;   stdUncW = 0.01;

% generate populations of std uncertainties for each 'realization' of the 'test'
uncT = (stdUncT) * rand ( numIts );    uncP = (stdUncP) * rand ( numIts );
uncR = (stdUncR) * rand ( numIts );    uncW = (stdUncW) * rand ( numIts);

For i = 1 To numIts              % perturb the surrogate experimental data
    T_perturb = T + uncT(i);     % and recalculate the result
    P_perturb = P + uncP(i);
    R_perturb = R + uncR(i);
    W_perturb = W + uncW(i);
    rho(i) = P_perturb / T_perturb / (R_perturb/W_perturb) ;
Next i

combinedStdUnc = stdev( rho );
```

In this example, `rand` represents a function call that generates an array of randomly distributed numbers with 0 mean and unit standard deviation. When multiplied by the appropriate standard uncertainty, the resulting population of random numbers has the proper scale and dimensional units of the standard uncertainty.

The random number generation can have any probability distribution appropriate to the measurand in question, although a Gaussian generator is normally used and was used for all results presented in this paper. The example above does not distinguish between error classifications. However, random and systematic uncertainty distributions can be generated separately using their respective standard uncertainties as scaling factors. In that case, both uncertainties are added to the surrogate data point in the perturbation loop. If correlated uncertainties can be estimated, they are simulated by adding the same random number to the two correlated variables on each iteration[20]. A similar technique is used when time-series data are being simulated[4]. In that case, an inner loop is created to represent each time step. A random uncertainty is added to the surrogate experimental data on each iteration of the inner loop, but the systematic uncertainty is added to the data only on each iteration of the outer loop. This simulates the same fixed bias (e.g., calibration error) that would exist on all of the time-series points but allows for appropriate perturbations due to random fluctuations (e.g., line noise) on the individual time-series points.

A Monte Carlo simulation does not rely on the linearizing approximations inherent in Eq. (1), nor does it require calculating the partial derivatives numerically. It is easier to implement in all but the simplest of cases. Even a deceptively simple data reduction equation can lead to difficulties deriving the standard uncertainty. Consider:

$$C_D = \frac{F_N}{q_\infty S} sin\alpha + \frac{F_A}{q_\infty S} cos\alpha \tag{4}$$

This equation for the drag coefficient appears as simple as Eq. (2) but in reality, the dynamic pressure is a function of the total and static pressure measurements, so implicit partial differentiation of q_∞ with respect to P_t and P_s is required when applying Eq. (1) to Eq. (4). The resulting algebraic expressions become very lengthy, as Ref. 18 shows for this specific example. In comparison, if the data reduction computer code already exists offline for Eq. (4) – with a subroutine to calculate q_∞ given P_t and P_s – it is simple in modern programming languages to wrap a Monte Carlo algorithm around it.

Another important advantage to Monte Carlo simulation techniques is for applications in which the data reduction equations do not exist in closed form and a closed-form approximation either is not possible or it fails to faithfully represent elements of interest in the uncertainty analysis. In the case of the NTF, a real gas equation of state is used, so the thermodynamic properties have to be calculated iteratively before q_∞ can be calculated and used in Eq. (4). A closed-form propagation equation for C_D uncertainty is therefore not possible without simplifying approximations. Other examples where a Monte Carlo approach is necessary include algorithms with branching logic, built-in regressions, assessing sensitivity to moving average and other digital filter settings, and evaluating data rejection algorithms[4,22].

C. Standard Uncertainties in the NTF Model

The NTF uncertainty model is programmed generically to propagate both random and systematic standard uncertainties for most of the data that are measured in a test. This includes the six balance forces and moments, the three basic thermodynamic measurements (total and static pressure and total temperature), the model attitude (pitch, roll, and yaw angles), weight tares, and so on. In the results presented later, only the most salient of these have been exercised. The available systematic error estimates are described in this section, but they have not been exercised in any of the results presented later. The random error estimates are based on test data; the methods used to estimate these are deferred to Section V after the test program has been described.

Although primary focus of the uncertainty model has been on estimating and propagating random errors, the current version of the model does simulate some of the more important systematic error sources. The NTF Flow Reference System (FRS) attempts to minimize uncertainty in P_t and P_s by providing the total and static pressures to the data system through combinations of absolute and differential measurements that depend on the magnitude of the differential pressure P_t - P_s [23]. A detailed model of the FRS has been incorporated into the uncertainty model using the vendor's stated elemental systematic uncertainties and an unpublished analysis[24] of recent as-found calibrations of the system. The model includes a correlated systematic uncertainty based on the assumption that the transducers are calibrated by the same standard. Because plans are in place to replace the FRS, a generic uncertainty model and a model based on another vendor's uncertainty statements are also incorporated in the model. These have

allowed a thorough analysis of the systematic uncertainty in Mach number, dynamic pressure, and Reynolds number, which will be incorporated into the specification for the new system.

Detailed calibration data sheets for NTF balances currently do not separate errors due to repeat loadings, curve fit residual errors, inherited standard uncertainty, etc., as suggested in the Ref. 25 recommended practice. This precludes a contribution analysis to determine the error sources that dominate the balance calibration uncertainty. However, the overall uncertainty statements for each component have been incorporated into the model.

Blockage corrections are available in the NTF, but they have not yet been incorporated into the offline data reduction code, and so are not available in the uncertainty model. However, Walker[10,26] has investigated the validity of the wall interference correction method used at NTF. In the process, he developed one of the very few rigorous uncertainty assessments ever to be undertaken for wall corrections. It should be possible without significant effort to incorporate those results into the model in the future.

V. Benchmark Tests to Establish Random Uncertainties

The uncertainty model development is part of a larger, ongoing effort to understand the sources of variability in the NTF and systematically address them as time and resources allow. As an initial part of that effort, the NTF's conventional check standard test was extended in several ways, as described next. It was then possible to use the data from these tests to estimate random uncertainties for the measured variables directly from these test data.

A. Test Program

Although the NTF is primarily a high Reynolds number test facility, it can and frequently does function as a standard transonic pressure tunnel; customers often require Reynolds number data from the NTF to compare to testing done at other facilities around the world. Results in both air and cryogenic modes are therefore of interest. The NTF check standard is the Pathfinder I transport model[16]. For the tests reported here, the NTF 113B balance was used. The Pathfinder I is representative of a subsonic, energy-efficient transport with a wide-body fuselage.

Table 1 shows the set of tunnel conditions selected for the tests. These conditions are representative of a large portion of stability and performance testing done at the NTF. They include low-speed conditions seen during high-lift configuration testing as well as high-speed conditions typical of commercial transport performance testing. The conditions shown are generally similar to the check standard testing used to generate the NTF process control charts such as Fig. 2. Check standard tests at NTF have historically been done only in air mode due to the high cost of cryogenic testing. In this case, cryogenic runs were also included. Mach number and dynamic pressure were held generally the same for these runs as for the air-mode runs, while using the cryogenic capability to elevate Reynolds number. (The Reynolds number in Table 1 is based on the mean chord length of the Pathfinder I, which is 5.74 in.) This ensured similar aero-elastic performance while also allowing a direct comparison of variability to the previous check standard tests.

Table 1. Tunnel Test Conditions

M_∞	P_t, psia	T_t, °F	Re_c x 10^6	q_∞, psf
Air Mode				
0.800	21.5	120	2.64	910
0.800	39.9		4.90	1691
0.189	50		1.87	176
0.289	50		2.80	398
0.500	113.5		10.30	2424
Cryogenic Mode				
0.800	21.5	-250	11.00	910
0.800	39.9		20.50	1691
0.189	50.0		7.60	176
0.289	50.0		11.40	398
0.820	59.0		30.53	2562

Run sets comprised four back-to-back pitch polars at each test condition. Each polar consisted of pitch-pause data points taken between -2 deg and +2 deg of pitch, in increments of 0.5 deg. All polars pitched from negative to positive angle of attack, but model roll alternated on each run, resulting in the following sequence of runs: upright, inverted, inverted, upright. This first and last of these constitutes a group in the SPC sense and is the same group definition currently used for NTF check standard tests (Fig. 2). The coupled upright and inverted runs were then used to calculate tunnel flow angularity in the normal way by comparing differences in C_N. Wind-off zeros were recorded at the beginning and end of each test condition to remove bias due to temperature drift in either the tunnel or control room.

Each polar took approximately 3 minutes to complete resulting in about 20 minutes at each condition in a series. The total time to complete a series was about 3.5 hours, including wind-off zeros, pressure system calibrations, and changing tunnel total pressure. Five air series were collected over a period of approximately 3 days during NTF

Test 193 in July 2008. During NTF Test 194 in September 2008, one air series was repeated followed by two cryogenic series. The latter series were run back-to-back with approximately 3 hours separating comparable runs.

Numerous auxiliary runs were made in both tests for various diagnostic purposes related to the effort at NTF to understand sources of variability. Most of these are outside the scope of this paper, but some were of use in assessing random uncertainties of measured data. For example, 60 seconds of continuous data were acquired at many of the conditions in Table 1 for -2, 0, and 2 deg pitch. The results could then be re-reduced to simulate different averaging times. These runs resulted in true back-to-back measurements that could be compared to the within-group measurements of comparable points in the two upright runs of a group.

B. Estimating Random Uncertainties at the Measurement System Level

Random uncertainties for measured variables are derived in some sense from observations[20] – repeat measurements, auxiliary tests over a representative time frame, previous test experience, etc. The benchmark test data have been used as described in the following subsections to derive random uncertainties at the measurement system level rather than the elemental level[18]. This means, for example, that the random uncertainty in total pressure is estimated by analyzing repeated total pressure measurements themselves, rather than attempting to estimate and combine elemental sources such as unsteady flow and freestream turbulence effects, orifice and transducer environment, power supply fluctuations, etc. Analysis at the measurement system level includes all such sources but cannot distinguish between them.

As noted above, five air series tests were conducted in NTF Test 193 (T193). For any one tunnel condition and model attitude (pitch and roll angles), this resulted in 10 nominally identical observations, or 20 such observations if no distinction is made between upright and inverted runs. For the two cryogenic series tests, there were only 8 nominally identical observations, even when upright and inverted runs are considered together. However, considerably more observations than this were used by accounting for or averaging through the influence of model attitude, as discussed below.

1. Freestream Measurements

The measurement systems that produce the calculated freestream Mach number, dynamic pressure, and Reynolds number are, of course, the total and static pressure, and total temperature. Thus, random uncertainties in the freestream conditions can be evaluated by propagating the random uncertainties in these measurements through the NTF data reduction equations. Initial evaluation of the variability in the freestream measurements showed a clear dependence on freestream dynamic pressure, but the scatter did not depend on the model attitude. Based on this initial analysis, the standard uncertainties for P_t, P_s, and T_t were simply calculated as the standard deviation of these measurements over the entire set of data at a particular total pressure and temperature setpoint. With 9 pitch angles per run, 4 repeat runs per series (2 upright, 2 inverted) at each dynamic pressure, and 5 series repeats for air mode, this results in 180 available observations. For cryogenic mode, 72 observations were available. In a few cases, the setpoint total pressure or temperature were not quite identical to the other runs. In those cases, the entire run was not discarded from the calculation, rather than attempting to normalize all of the data sets, because there were still plenty of observations available to calculate the standard deviations.

Total temperature showed no trend with dynamic pressure, so the average standard deviation over all dynamic pressure setpoints was used to calculate the random uncertainty. For total and static pressure, there was a clear correlation in most cases with the dynamic pressure. The uncertainties (with coverage factor 2) and regressions used in the Monte Carlo simulation are shown in Fig. 3, plotted against dynamic pressure. The trends in tunnel conditions are qualitatively typical of what was described by Hemsch et al. [9], although they were referring to balance repeatability: at lower dynamic pressures, the uncertainty remains about the same, but after some threshold value, it begins to increase with dynamic pressure. For total and static pressure in cryogenic mode, the threshold appears to be around q_∞ = 400 psf. It is much higher for total pressure in air, as shown in the plot.

The plots in Fig. 3 show two sets of data along with the regression curves. Only the main data set (diamond symbols) were used to generate the regressions. The second data set consists of 36 back-to-back points, which were taken from the 60-second continuous data samples described above. The 60, 1-second samples were acquired at -2, 0, and +2 deg of model pitch, resulting in 180 sequential samples. These were re-calculated as 5-s averages at each pitch angle, for a total of 36 points. The resulting standard deviation of these 36 points (with coverage factor 2) is shown in the plots for comparison to the main data sets, which were obviously acquired over a longer time frame (hours and days compared to 3 minutes). It is interesting that the trends between variability in the two data sets are similar – within-run repeatability and between-group repeatability are comparable in magnitude by this measure.

The final points of interest to note in Fig. 3 are that the magnitudes of the uncertainty in total pressure are about the same between cryogenic and air mode operation, whereas the static pressure uncertainty in cryogenic mode is

significantly higher than in air mode. Also, the static pressure uncertainties in both modes are significantly higher than the total pressure uncertainties.

2. Balance Measurements

Slight differences in flow angularity between runs result in a different angle of attack, which in turn produces wide variations in F_A and F_N even when C_D or C_L vary much less. As some of the variation in F_A and F_N is of course physically meaningful (and certainly not random), it is inappropriate in the case of balance measurements to consider points as 'nominally identical' between runs even when they have common pitch angle and tunnel condition setpoints. However, it is more reasonable to assume that flow angularity does not change over the relatively short time span between the first and last upright run at a particular dynamic pressure setpoint. This was verified by calculating flow angularity from both the first pair and second pair of upright/inverted runs. The differences were always small between these two but not necessarily between runs or series. If flow angularity dependence is considered negligible over such short time spans, a simplistic residual analysis allows the variability in balance measurements to be compared between runs. For a particular tunnel condition and pitch angle setpoint in a series, the following differences were calculated:

$$\begin{aligned} \Delta F_{A1} &= F_{A1} - (F_{A1} + F_{A4})/2 \\ \Delta F_{A4} &= F_{A4} - (F_{A1} + F_{A4})/2 \end{aligned} \tag{5}$$

In this equation, F_{A1} is the axial force in the first run of the sequence, and F_{A4} is the axial force in the fourth run (second upright run). The residuals are equal and opposite. They represent a crude estimate of the variability between the two runs. A similar pair of residuals was calculated for the inverted runs that occurred between these two upright runs. With the series repeat runs (5 for air, 2 for cryogenic), this resulted in 20 and 8 data points, respectively, for comparison at one dynamic pressure and pitch angle setpoint.

The standard deviations of these residuals were calculated and compared between pitch angle settings. Most of the resulting standard deviations showed no obvious trend with pitch. (In some cases, particularly lower dynamic pressures, the standard deviation was higher at the extreme pitch angle settings.) To avoid a two-dimensional regression (balance uncertainty vs. dynamic pressure and pitch angle), the standard deviations were averaged across all 9 pitch angles to arrive at the standard uncertainties for the balance forces. Instead of averaging standard deviations from individual pitch angles, an alternative approach of calculating the standard deviation of all residuals (all pitch angles, all repeats) gave similar results.

The random uncertainties calculated in this way are shown for axial and normal force in Fig. 4. As in Fig. 3, only the main data sets were used to calculate the uncertainties; the standard deviations (with coverage factor 2) of the back-to-back measurements are shown only for comparison. The back-to-back plots are from the same runs as in Fig. 3, except they are calculated from 1-second averages instead of 5-second averages.

As in Fig. 3, a strong correlation between balance variation and dynamic pressure is obvious. In this case, however, there doesn't appear to be a threshold below which the uncertainties are independent of dynamic pressure – or if it exists, it is a low value. The uncertainty in cryogenic mode is between 1.5 and 2 times higher than in air mode for both axial and normal force over most of the dynamic pressure range. Also shown for reference are the overall calibration (systematic) uncertainties for the NTF 113B balance. For the axial force, the observed random uncertainty falls below the calibration uncertainty at all dynamic pressures. The normal force random uncertainty exceeds the calibration uncertainty for about $q_\infty \geq 600$ psf in both air and cryogenic modes.

Strong correlation with dynamic pressure was also observed in the other forces and moments (not shown). The pitching moment and side force tended to increase the most with dynamic pressure. The yawing and rolling moments were correlated with dynamic pressure but did not increase nearly as much over the dynamic pressure range tested.

The variation of the freestream properties during a single run was not always random. In several back-to-back run sets we looked at in detail, total pressure appeared to be randomly distributed during the run, but static pressure decreased consistently by about 2 psf from the beginning of the run to the end, and the Mach number increased consistently by about 0.001. Considering the correlation of both balance forces and tunnel properties with dynamic pressure, the question was asked whether their random uncertainties are also correlated. Plots of F_A vs. P_s from high-speed (100 Hz) auxiliary data showed a 'shotgun blast' distribution. Figure 5 supports the lack of correlation. Using the high-speed data set, the cross-correlation coefficient function[27] was calculated for axial force and static pressure. Perfect correlation would be indicated by values of ±1, which is not the case in Fig. 5. A similar lack of

correlation was observed between other balance components and the static and total pressures. The in-run trends observed may instead be related to slight changes in wall interference during the pitch polar.

3. Model Attitude and Flow Angularity

The uncertainty in model pitch angle was estimated with the aid of auxiliary high-speed (100 Hz) time traces of the pitch angle feedback, which had been low-pass filtered at 0.4 Hz. At each setpoint, the standard deviation was calculated from the final 2 seconds of data prior to a setpoint change. As there was no obvious trend with pitch angle setpoint, the standard uncertainty at a particular dynamic pressure was taken as the average of the 9 pitch angle standard deviations. Because similar high-speed roll angle data were not available, the roll angle uncertainty was assumed to be the same as pitch angle uncertainty. The pitch angle random uncertainty is shown in Fig. 6 for air and cryogenic modes. Correlation with dynamic pressure is obvious, but it is strong only in cryogenic mode.

The random uncertainty in flow angularity was calculated using Hemsch's[28] analysis for repeatability over a time frame comparable to this test:

$$\begin{aligned} u_{Flow\ Angle} &= 0.633/q_\infty \text{ deg} && q_\infty < 290 \text{ psf} \\ &= 0.00218 \text{ deg} && q_\infty \geq 290 \text{ psf} \end{aligned} \tag{6}$$

4. Closing Comments on Estimating Random Uncertainties

The benchmark tests presented in this paper serve as a very good starting point for estimating random uncertainties in the NTF, but they are obviously limited to a single test article, with admittedly crude techniques used in some cases to arrive at the uncertainties. Going forward, future benchmark tests and customer test data can be used to refine these estimates and scale them[9,14,28] for other balances and model sizes. In addition, the completed model requires full implementation of the NTF systematic uncertainties so that in addition to repeatability and reproducibility, they can also properly compare their results to other simulations (i.e., other wind tunnels, prototype tests, and numerical tests).

VI. Results

The random uncertainties described above for the six balance components, three freestream measurement properties, model attitude angles, and flow angularity, were propagated through the uncertainty model using the appropriate data from representative runs in Table 1. For brevity, results in this section are confined mainly to M_∞ and C_D.

A. Random Uncertainty Propagation in the Freestream Properties

Figures 7 and 8 compare the calculated uncertainties in Mach number and dynamic pressure to the direct observations from the test data. As with the pressure data, the observed variations used data from all runs and model attitudes, under the assumption that the latter do not influence freestream properties. The agreement between the calculations and observations is reasonable in most cases, especially for dynamic pressure uncertainty, but the calculations are somewhat pessimistic at the lower Mach numbers in some cases. It is interesting that the uncertainty in Mach number increases with increasing dynamic pressure in cryogenic mode, but it decreases in air mode after q_∞ = 600 psf. We note from Table 1, however, that in the cryogenic case (Fig. 7b), the Mach number and dynamic pressure increase together, so the highest uncertainty corresponds to both maximum dynamic pressure and Mach number. In the air mode case (Fig. 7a), the highest uncertainty occurs in at the middle two dynamic pressures, both of which correspond to the highest Mach number tested in air mode.

Figure 9 shows the contributions of P_t, P_s, and T_t to the Mach number random uncertainty. A contribution analysis is calculated by running the simulation with all uncertainty sources set to zero except the one(s) of interest. As shown in the figure, the static pressure uncertainty dominates the Mach number uncertainty at the higher dynamic pressures. Considering that the components add as root-sum-squares to arrive at the combined result, the total pressure uncertainty is completely negligible except at the lowest dynamic pressures. The results for dynamic pressure uncertainty (not shown) exhibit the same trends as Mach number. This is perhaps not surprising in view of the relative magnitudes of the static and total pressure uncertainties in Fig. 3. This result leads to the conclusion that any attempt to improve the Mach number variation would need to focus on understanding and minimizing the static pressure variation.

B. Random Uncertainty Propagation in the Axial Force and Drag Coefficients

Figure 10 compares results from a variety of sources to quantify the variation in the axial drag coefficient. Shown are results from the uncertainty propagation simulation, the NTF benchmark tests, SPC results from Hemsch et al.[9], sequential measurements and RSA calculations from the present work, and RSA calculations from Wahls et al.[11] All of the data sets are from the Pathfinder I model except those of Wahls et al. Their results were for a 767 model; the error bars denote the range of results they obtained from various model configuration changes during the test.

Some clarification may be in order regarding the inclusion of both between-group and within-group variation in Fig. 10. Hemsch et al. [9] defined their group as three back-to-back upright runs. Their between-group variation was calculated on the basis of a series of runs made during a single tunnel entry and over a time frame similar to the time frames of the tests in the present work. The NTF check standard SPC charts define a group similarly – as two upright runs, one before and one after two intervening inverted runs. However, the calculation of between-group variation for the NTF SPC charts includes not only runs made over short time frames (hours up to several days), but also over multiple installations. In attempting to assess variation over a comparable time frame, it seems to make more sense to use within-group variation from the NTF SPC charts for comparison with both the Monte Carlo simulation results and the between-group results of Hemsch et al.

The agreement between the different methods in Fig. 10 is quite good, particularly between the NTF check standard results, the results of Hemsch et al., and the propagation results. Considering the confidence limits on the standard deviation[9,20] for a Normal distribution (that is to say, the uncertainty of the uncertainty), the SPC and uncertainty results are effectively the same in Fig. 10. Not surprisingly, the RSA results exhibit more inconsistency than the more rigorous methods.

Figure 11 shows the random uncertainty in the drag coefficient with increasing dynamic pressure for both air and cryogenic modes. Only RSA data are available for comparison in this case as SPC tests have not historically been done in the NTF; recall as well that the results of Wahls et al.[11] are from a different model. The trends in the uncertainty propagation are similar in both cases. For air, however, the uncertainty levels out and becomes independent of dynamic pressure, whereas it begins to increase in the cryogenic case. This is not particularly surprising in view of the results in Figs. 3, 4, and 6 where the rate of increase with dynamic pressure in most of the component uncertainties is much higher in cryogenic mode than air mode.

Figure 12 shows the contribution from the various sources to the combined random uncertainty at selected pitch angle and dynamic pressure setpoints. Air mode results are on the left and cryogenic mode results are on the right. The relative contributions are generally not very different between the air and cryogenic modes, only the levels. This is comforting at some level, because it suggests that the behavior of the measurement systems and probably the tunnel and model, are not fundamentally different in the two modes of operation. In all cases, axial force uncertainty, not unexpectedly, is a dominant contributor, but it is not necessarily the only important one. At the lowest dynamic pressure in air mode (Fig. 12a), the uncertainty contribution from the freestream measurements is the same as the axial force contribution. At the highest cryogenic dynamic pressure (Fig. 12f), axial force, normal force, and pitch angle uncertainties all contribute equally at the highest angle of attack. Generally, however, only the normal force uncertainty is an equal and in some cases larger contributor than the axial force. Taken together, the results in Fig. 12 suggest that if an improvement in drag coefficient random uncertainty is sought, focusing on axial force uncertainty alone would not be sufficient.

The uncertainties in balance forces, pitch angle, and even the freestream tunnel conditions all exhibit increasing magnitudes and generally strong correlation with increasing dynamic pressure and Reynolds number, which propagates into the calculated uncertainties for the freestream properties and the drag coefficient. This may point to an aeroacoustic or aeroelastic interaction with the model or model support system, although this is speculative on the basis of the data set that was acquired in the test program reported here. However, vibration problems related to such phenomena have been observed previously in the NTF[29,30] and have been found to be magnified at high Reynolds number (cryogenic) conditions.

VII. Concluding Remarks

Unprecedented levels of product performance requirements are driving design decisions and product costs on the basis of ever-smaller observations of performance increments. This environment dictates the requirement for high-fidelity wind tunnel data, even from wind tunnels that were put into operation decades ago. The need for accurate and precise wind tunnel results in turn drives the need for ongoing improvement in wind tunnel data quality. Tools

and resources are needed that not only assess the data quality but also provide a technical basis to justify specific improvement initiatives.

An uncertainty propagation model based on a Monte Carlo technique has been developed for the NTF. This approach provides a drill-down capability to identify the relative influence of the uncertainties in measured data (e.g., total pressure) on the uncertainties of the calculated data (e.g., Mach number and drag coefficient) provided to the customer. It was shown that the tool is complementary to the more fundamental but high-level information provided by SPC. The model has been populated with initial estimates of random errors for the most salient measured parameters. The estimates are based on benchmark tests in both air and cryogenic mode, which were conducted as part of this project.

Analysis of the benchmark test data showed that random uncertainties in the measured parameters – tunnel pressures, balance forces, and model pitch angle – were correlated with the tunnel's dynamic pressure and increased with it. Further, the rate of increase was higher (and the correlation stronger) in cryogenic (high Reyolds number) mode than in air mode. The results of the uncertainty propagation showed that the uncertainties in both calculated Mach number and dynamic pressure are driven by the uncertainty in measured static pressure, while the uncertainty in drag coefficient is driven by both axial and normal force uncertainty.

It was speculated that some of the increase in uncertainty as dynamic pressure and Reynolds number increase could be related to aeroacoustic or aeroelastic interactions with the model or model support system. Although the data set described in this paper was not sufficient to investigate this, vibration phenomena have been observed in previous studies and found to be magnified at higher Reynolds numbers. The solutions developed or suggested previously to mitigate vibration phenomena generally focused on safe operation and avoiding restrictions to the testing envelope. As improvements in data quality are sought due to new, customer-driven performance requirements, a return of focus to further refine previous solutions would seem an appropriate path. This a common approach in continuous improvement initiatives – a solution that was once sufficient must be revisited in view of new customer requirements. The metric of success for such activities in this case would shift from health monitoring to reducing data variability. As indicated in the results presented in this paper, reducing the random uncertainties in static pressure and in the normal and axial forces would have the largest impact on the Mach number and drag coefficient variability.

Acknowledgments

The authors are grateful for helpful discussions with many past and present NTF staff members and customers, notably Mr. Allen Kilgore and Dr. Eric Walker (NASA Langley) and Mr. Dale Belter (Boeing). Thanks go to Mike Acheson (NASA Langley) and Jim Wright (Jacobs ROME), who ported the data reduction code to Matlab – and in some cases rewrote it completely. Tony Nagle (Jacobs Technology Group) vectorized the Matlab code and also implemented some of the real-gas calculations for the freestream properties. Thanks are also due to Jacobs technical and senior management: Dr. Steve Dunn, Brant Adams, Rogers Starr, and especially to Shawn McDonald, for shepherding (cat-herding) resources to work on this project.

References

[1]Hemsch, M.J., "Development and Status of Data Quality Assurance Program at NASA Langley Research Center – Toward National Standards," AIAA Paper No. 96-2214, 1996.

[2]Belter, D., "Comparison of Wind-Tunnel Data Repeatability with Uncertainty Analysis Estimates," AIAA Paper No. 98-2714, 1998.

[3]Ulbrich, N., and Boone, A.R., "Uncertainty Analysis of the Test Data in the Ames 11-Foot Transonic Wind Tunnel," AIAA Paper No. 2004-2195, 2004.

[4]Walter, J.A., Canacci, V., *et al.*, "Uncertainty Analysis of Aerodynamic Coefficients in an Automotive Wind Tunnel," SAE Paper No. 2005-01-0870, 2005.

[5]Fuller, D.E., "Guide for Users of the National Transonic Facility," NASA Technical Memorandum 83124, July, 1981.

[6]Campbell, J.F., "The National Transonic Facility – A Research Perspective," AIAA Paper No. 84-2150, 1984.

[7]McKinney, L.W., Bruce, W.E., and Gloss, B.B., "National Transonic Facility Status," *Transonic Symposium: Theory, Application and Experiment, Volume 2 p 1-39 (SEE N91-24132 16-02*, 1989. Also available at ntrs.nasa.gov.

[8]Gloss, B., and Bruce, R., "A Solution to Water Vapor in the National Transonic Facility," AIAA Paper No. 89-0152, 1989.

[9]Hemsch, M.J., Tuttle, D.G., Houlden, H.P., and Graham, A.B., "Measurement of Force Balance Repeatability and Reproducibility in the NTF," AIAA Paper No. 2004-0771, 2004.

[10]Walker, E.L., "Validation of Blockage Interference Corrections in the National Transonic Facility (Invited)," AIAA Paper No. 2007-0750, 2007.

[11]Wahls, R.A., Adcock, J.B., Witkowski, D.P., and Wright, F.L., "A Longitudinal Aerodynamic Data Repeatability Study for a Commercial Transport Model Test in the National Transonic Facility," NASA Technical Paper 3522, August, 1995.

[12]Mineck, R.E. and Pendergraft, O.C., "Test-to-Test Repeatability of Results From a Subsonic Wing-Body Configuration in the National Transonic Facility," NASA Technical Memorandum 2000-210079, March, 2000.

[13]Press, W.H., Teukolsky, S.A., Vetterling, W.T., and Flannery, B.P., *Numerical Recipes in C*, 2nd Ed., Cambridge University Press, 1992, Chapter 15.

[14]Hemsch, M., Grubb, J., Krieger, W., and Cler, D., "Langley Wind tunnel Data Quality Assurance – Check Standard Results," AIAA Paper No. 2000-2201, 2000.

[15]Montgomery, D.C., *Introduction to Statistical Quality Control*, 5th ed., John Wiley & Sons, Inc., 2005.

[16]Jacobs, P.F., and Gloss, B.B., "Longitudinal Aerodynamic Characteristics of a Subsonic, Energy-Efficient Transport Configuation in the National Transonic Facility," NASA Technical Paper 2922, 1989.

[17]International Organization for Standardization, *Guide to the Expression of Uncertainty in Measurement*, ISBN 92-67-10188-9, 1993 (Corrected and Reprinted, 1995).

[18]American Institute of Aeronautics and Astronautics, *Assessment of Experimental Uncertainty with Application to Wind Tunnel Testing*, AIAA Standard S-071A-1999, 1999.

[19]Moffat, R.J., "Describing the Uncertainties in Experimental Results," *Experimental Thermal and Fluid Science*, Vol. 1, No. 1, 1988.

[20]Coleman, H.W. and Steele, W.G., *Experimentation and Uncertainty Analysis for Engineers*, 2nd Ed., John Wiley and Sons, Inc., 1999.

[21]Foster, J.M., and Adcock, J.B., "User's Guide for the National Transonic Facility Research Data System," NASA Technical Memorandum 110242, 1996.

[22]Walter, J.A., Pruess, D.J., and Romberg, G.F., "Coastdown/Wind Tunnel Drag Correlation and Uncertainty Analysis," SAE Paper No. 2001-01-0630.

[23]Juanarena, D.B., Klaser, H.N., and Fuykschot, P.H., "The Flow Reference System – An Air Data System for Windtunnels," *International Congress on Instrumentation in Aerospace Simulation Facilities*, Wright-Patterson Air Force Base, 18-21 July 1995, pp. 40/1 – 40/14.

[24]Taylor, J.T., "Analysis of the Out-of-Tolerance Calibrations at NASA Langley Research Center," February, 2010 (unpublished). Available from the authors.

[25]American Institute of Aeronautics and Astronautics, *Calibration and Use of Internal Strain-Gage Balances with Application to Wind Tunnel Testing*, AIAA Recommended Practice R-091-2003, 2003.

[26]Walker, E.L., "Statistical Calibration and Validation of a Homogeneous Ventilated Wall-Interference Correction Method for the National Transonic Facility," NASA TP 2005 213947, 2005.

[27]Bendat, J.S., and Pierson, A.G., *Random Data Analysis and Measurement Procedures*, 3rd Ed., John Wiley and Sons Inc., 2000.

[28]Hemsch, M.J., "Analysis of Flow Angularity Repeatability Tests in the NTF," AIAA Paper No. 2006-0518B, 2006.

[29]Young, C.P., Popernack, T.G., and Gloss, B.B., "National Transonic Facility Model and Model Support Vibration Problems," AIAA Paper No. 90-1416, 1990.

[30]Edwards, J.W., "National Transonic Facility Model and Tunnel Vibrations," AIAA Paper No. 97-0345, 1997.

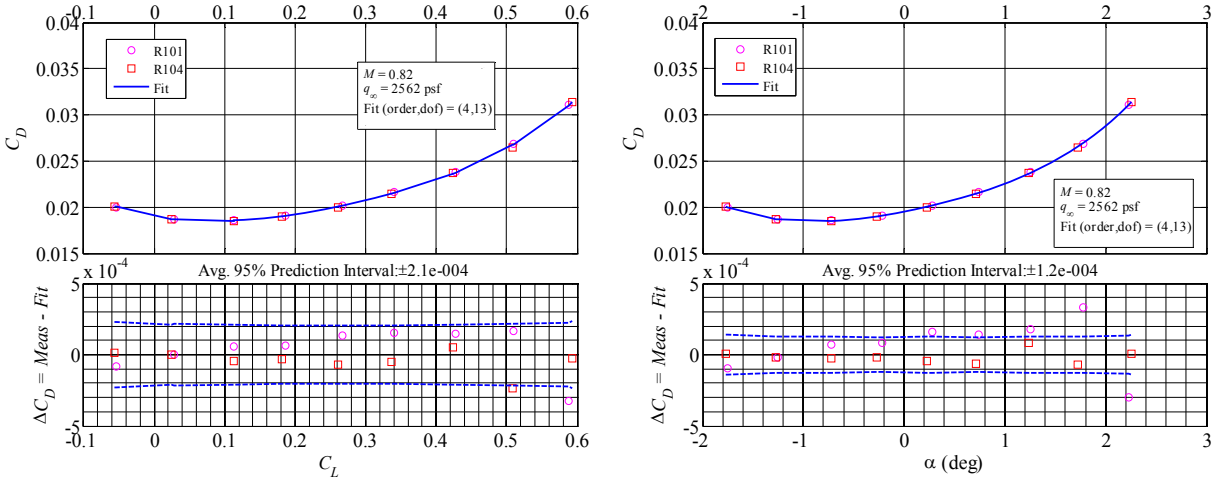

a) C_D regressed against C_L b) C_D regressed against α

Figure 1. Example RSA results.

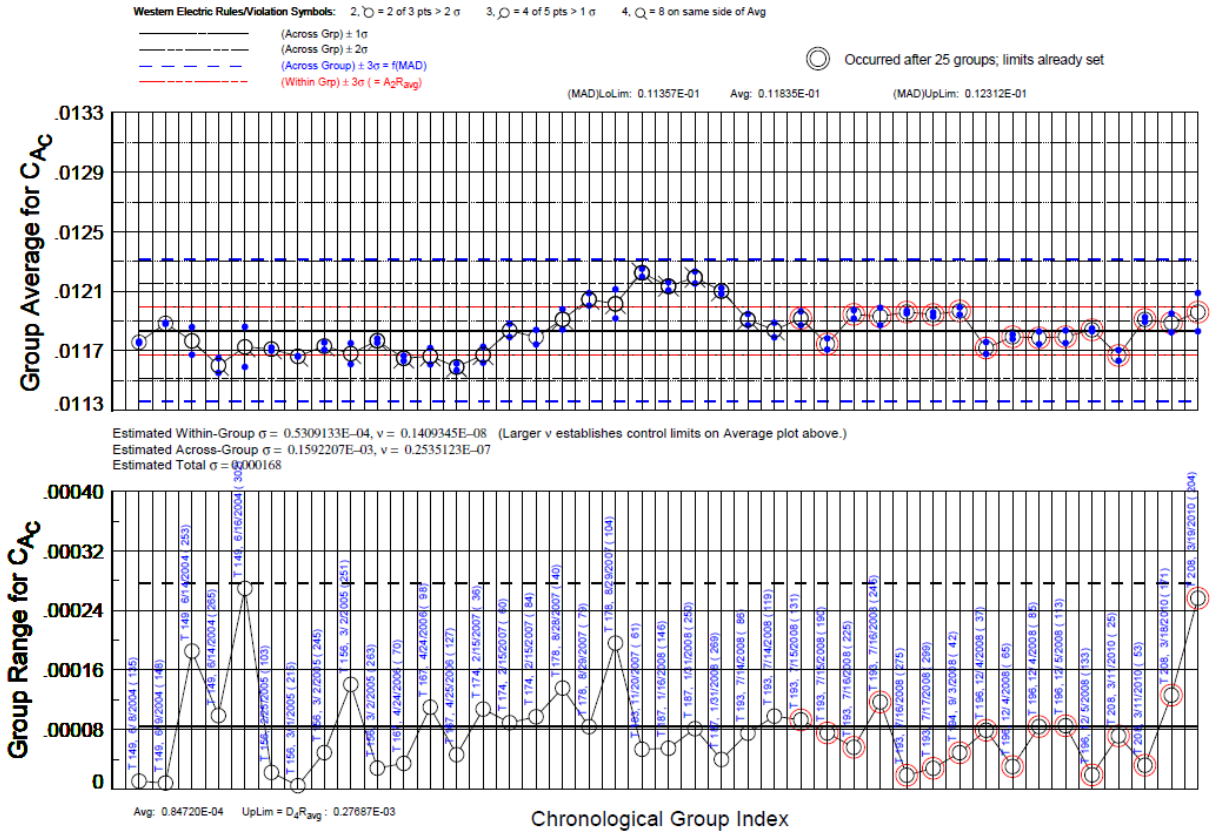

Figure 2. NTF Statistical Process Control chart for C_A upright, q_∞ = 1690 psf, M_∞ = 0.80, α= 2 deg, air mode operation.

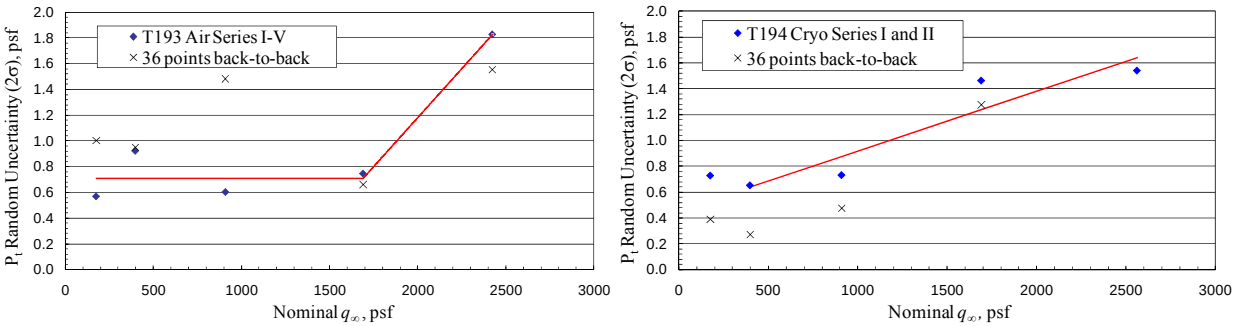

a) total pressure – air mode

b) total pressure – cryogenic mode

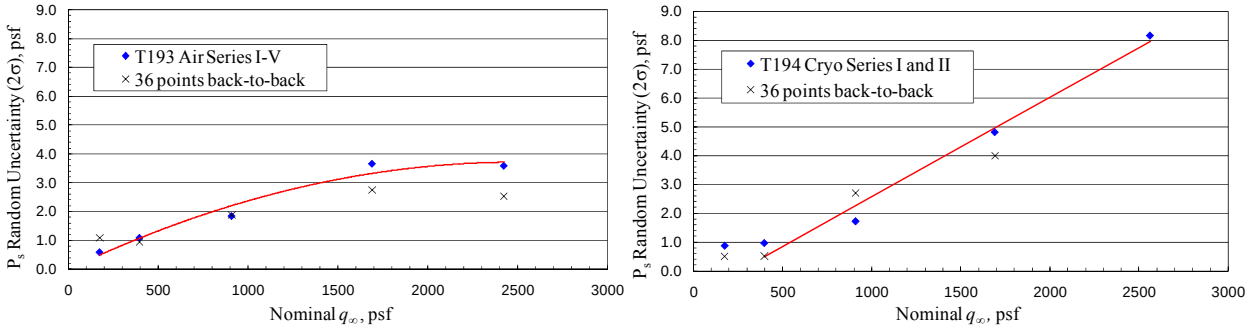

c) static pressure – air mode

d) static pressure – cryogenic mode

Figure 3. Random uncertainties for P_t and P_s estimated from measured data.

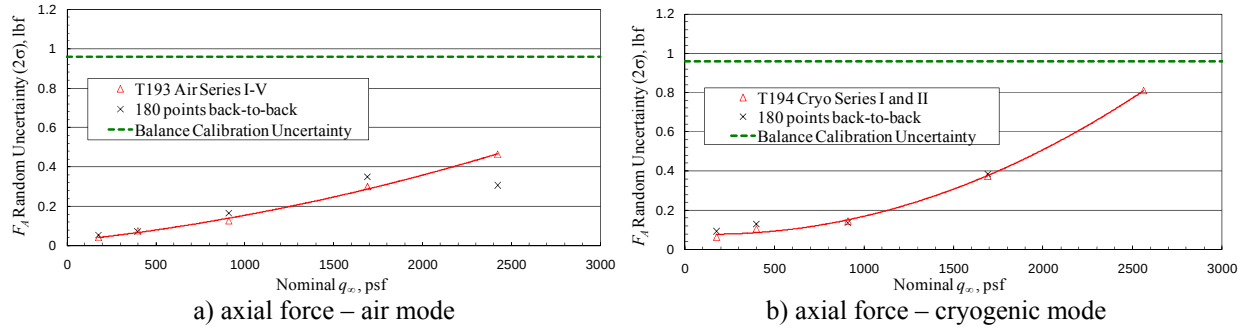

a) axial force – air mode

b) axial force – cryogenic mode

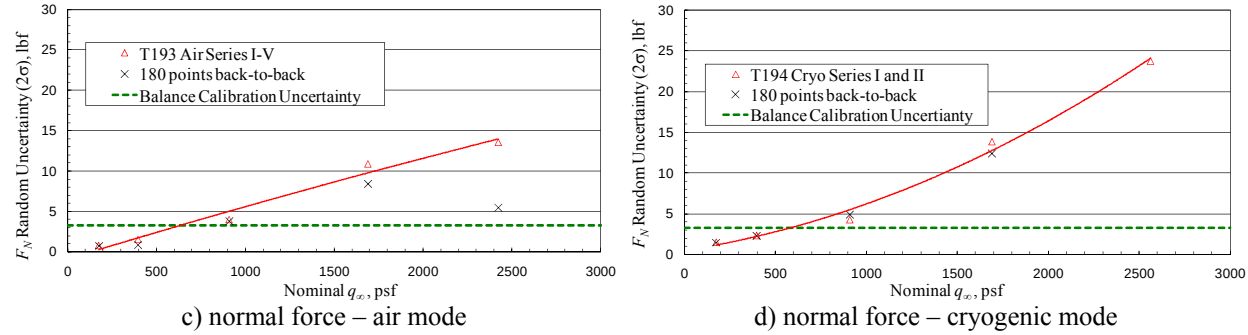

c) normal force – air mode

d) normal force – cryogenic mode

Figure 4. Random uncertainties estimated from measured balance data.

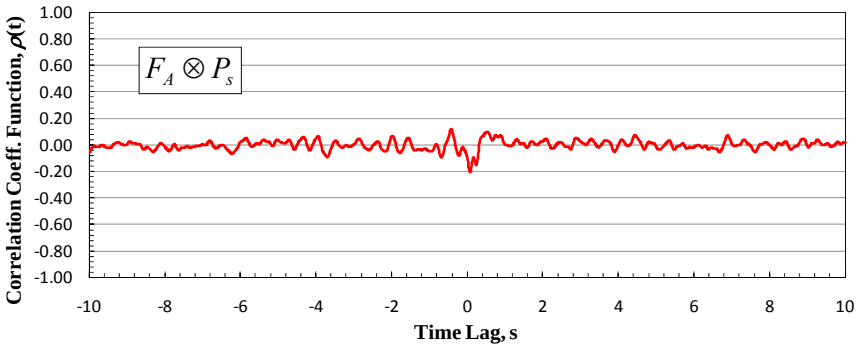

Figure 5. Cross-correlation coefficient function – static pressure and axial force (M_∞ = 0.8, q_∞ = 1691 psf, cryogenic mode).

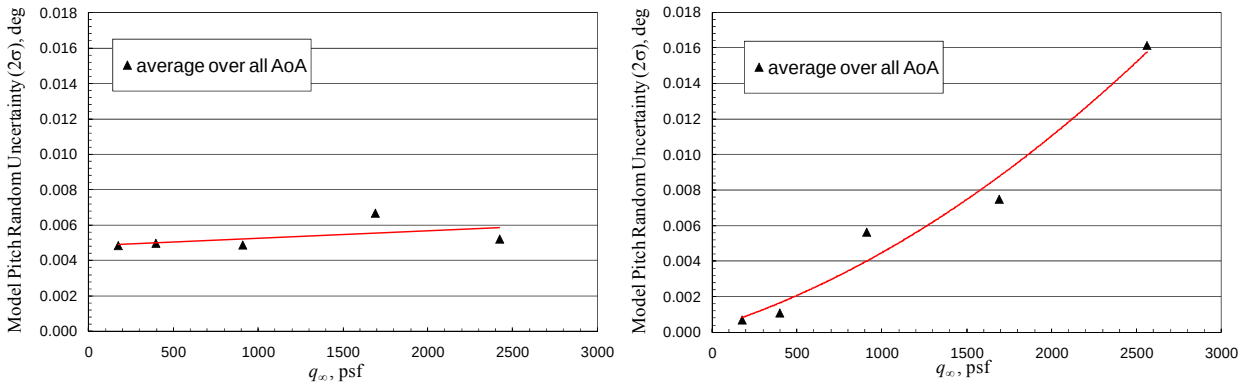

a) air mode b) cryogenic mode

Figure 6. Random uncertainty in model pitch angle.

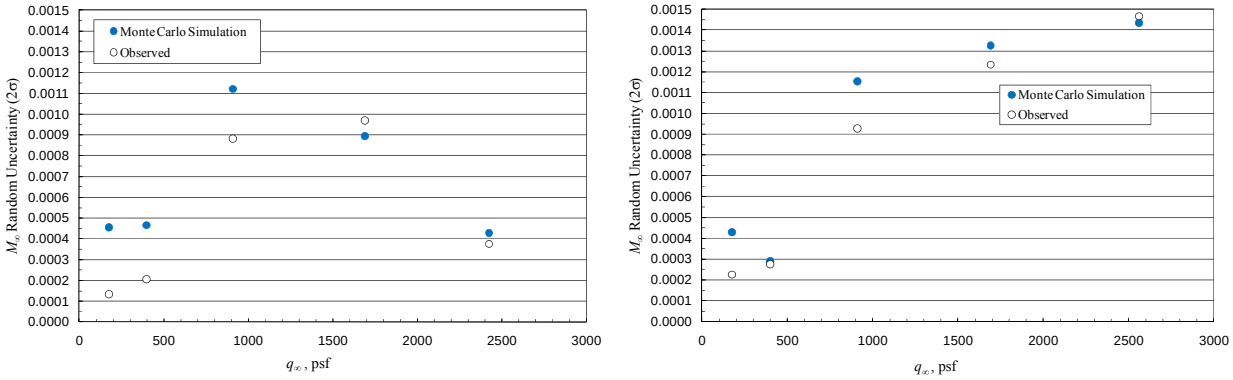

a) air mode b) cryogenic mode

Figure 7. Calculated vs. observed random uncertainty in M_∞.

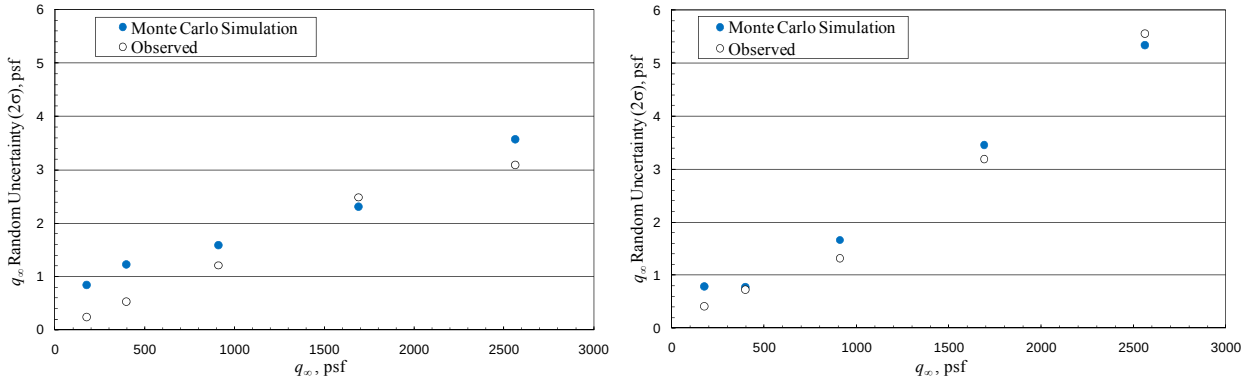

a) air mode b) cryogenic mode

Figure 8. Calculated vs. observed random uncertainty in q_∞.

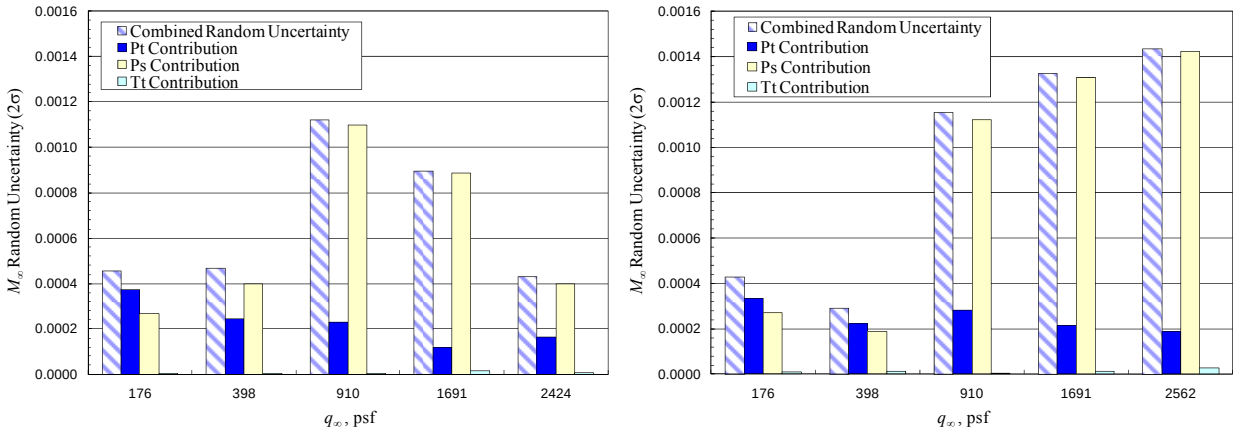

a) air mode b) cryogenic mode

Figure 9. Random uncertainty drill-down for M_∞ Note that component uncertainties add as root-sum-squares for the combined result.

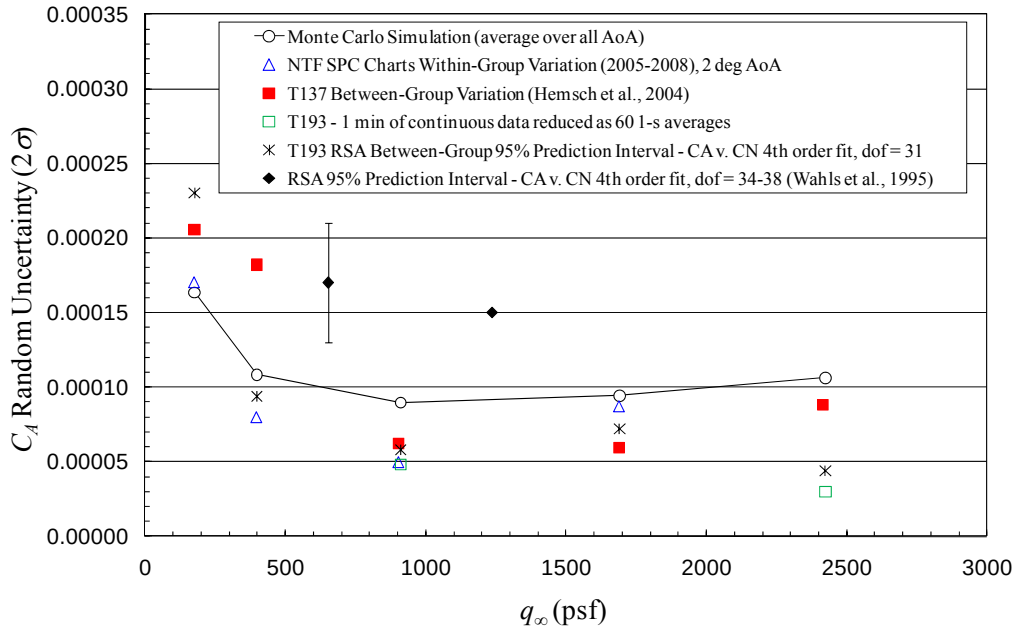

Figure 10. Air-mode variability in C_A.

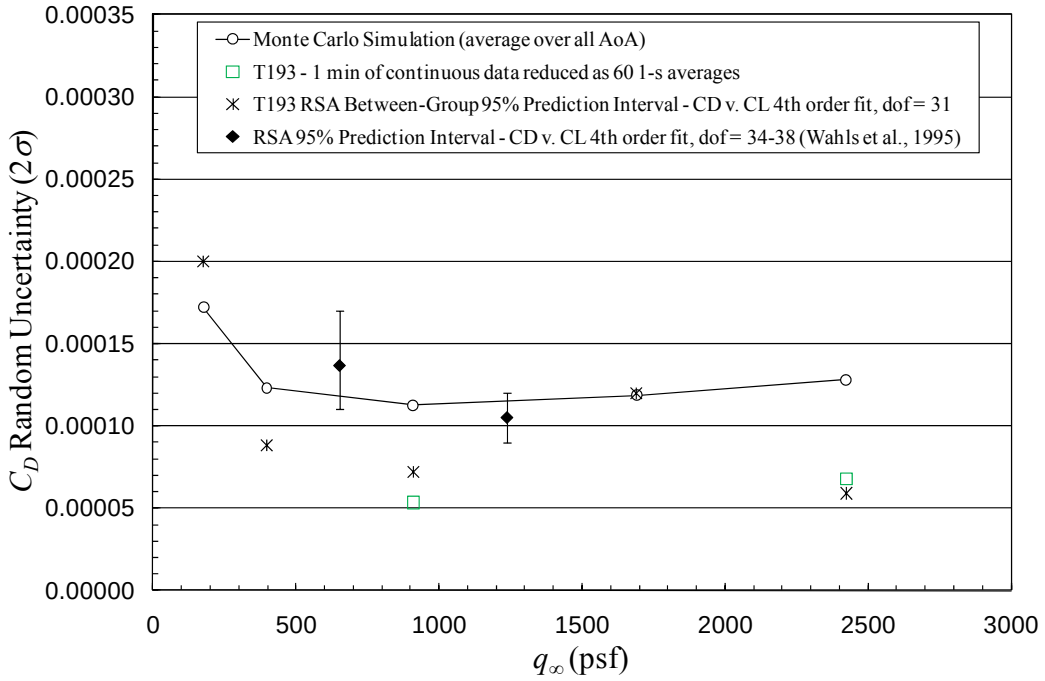

a) air mode

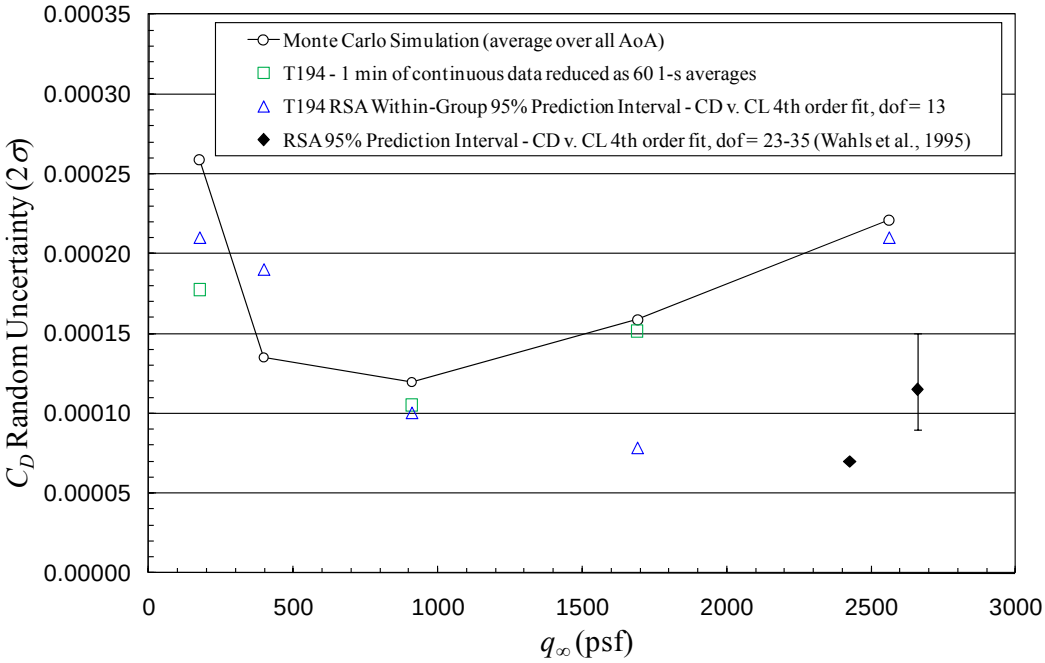

b) cryogenic mode

Figure 11. Random uncertainties in C_D.

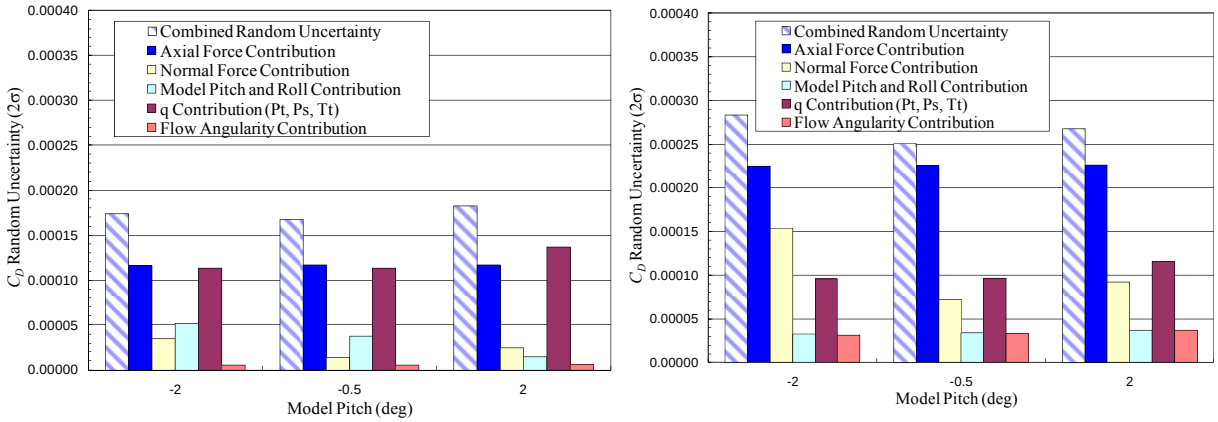

a) $M_\infty = 0.189$, $q_\infty = 176$ psf – air mode

b) $M_\infty = 0.189$, $q_\infty = 176$ psf – cryogenic mode

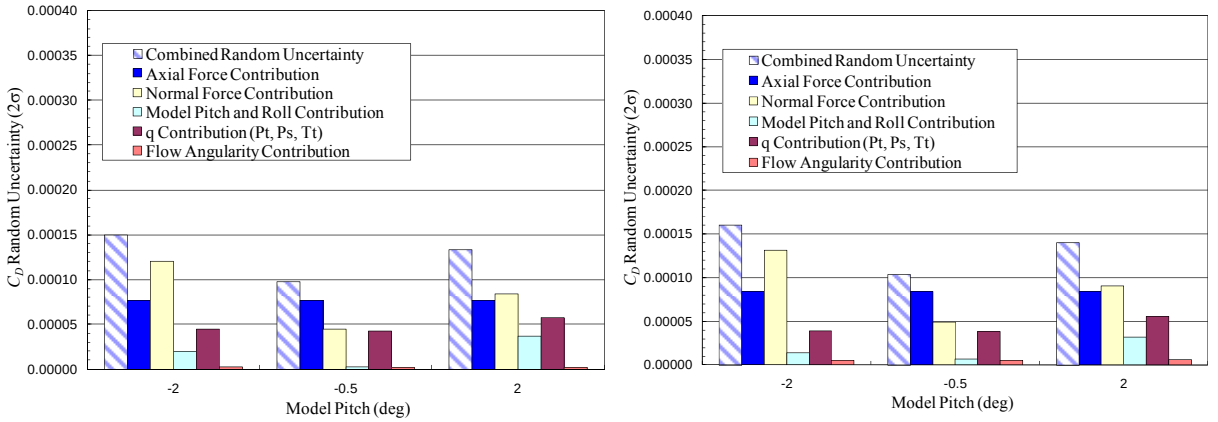

c) $M_\infty = 0.80$, $q_\infty = 910$ psf – air mode

d) $M_\infty = 0.80$, $q_\infty = 910$ psf – cryogenic mode

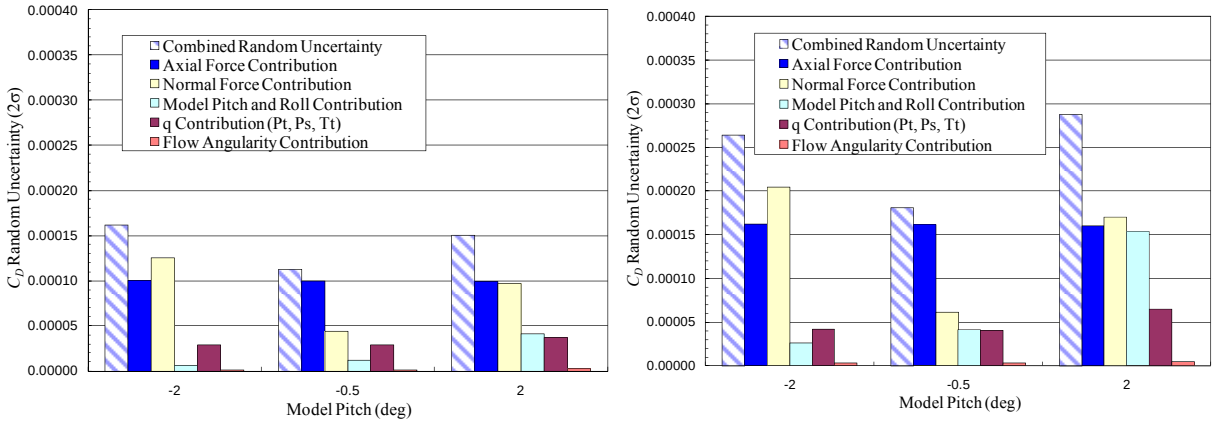

e) $M_\infty = 0.50$, $q_\infty = 2424$ psf – air mode

f) $M_\infty = 0.82$, $q_\infty = 2562$ psf – cryogenic mode

Figure 12. Uncertainty drilldown for C_D. Note that component uncertainties add as root-sum-squares for the combined result.